

Running of fermion observables in non-supersymmetric SO(10) models

Tommy Ohlsson^{a,b,c} and Marcus Pernow^{a,b}

^a*Department of Physics, School of Engineering Sciences,
KTH Royal Institute of Technology, AlbaNova University Center,
Roslagstullsbacken 21, SE-106 91 Stockholm, Sweden*

^b*The Oskar Klein Centre for Cosmoparticle Physics, AlbaNova University Center,
Roslagstullsbacken 21, SE-106 91 Stockholm, Sweden*

^c*University of Iceland, Science Institute,
Dunhaga 3, IS-107 Reykjavik, Iceland*

E-mail: tohlsson@kth.se, pernow@kth.se

ABSTRACT: We investigate the complete renormalization group running of fermion observables in two different realistic non-supersymmetric models based on the gauge group SO(10) with intermediate symmetry breaking for both normal and inverted neutrino mass orderings. Contrary to results of previous works, we find that the model with the more minimal Yukawa sector of the Lagrangian fails to reproduce the measured values of observables at the electroweak scale, whereas the model with the more extended Yukawa sector can do so if the neutrino masses have normal ordering. The difficulty in finding acceptable fits to measured data is a result of the added complexity from the effect of an intermediate symmetry breaking as well as tension in the value of the leptonic mixing angle θ_{23}^l .

KEYWORDS: Beyond Standard Model, GUT

ARXIV EPRINT: [1804.04560](https://arxiv.org/abs/1804.04560)

Contents

1	Introduction	1
2	Description of the minimal and extended models	2
2.1	SO(10) Lagrangians	3
2.2	Pati-Salam Lagrangians	3
2.3	SM-like Lagrangian	4
3	Parameter-fitting procedure	6
4	Results and discussion	8
5	Summary and conclusions	12

1 Introduction

Grand unified theories provide an intriguing framework for physics beyond the Standard Model (SM). The SO(10) gauge group is a popular version since it accommodates all SM fermions and the right-handed neutrino in one representation [1, 2]. However, in order to be a viable candidate, it must be able to reproduce the experimentally measured fermion masses and mixing parameters. Therefore, it is relevant to analyze how well the parameter values of a particular model can be fitted to the measured observables.

The issue of fermion masses and mixing parameters in non-supersymmetric (non-SUSY) SO(10) frameworks has been extensively discussed previously in the literature, see for example refs. [3–9]. The most minimal choice of scalar representations in the Yukawa sector of the Lagrangian that can reproduce the desired fermion data are the $\mathbf{10}_H$ and $\overline{\mathbf{126}}_H$ representations, which has been demonstrated in a number of previous fits [10–15]. One can also choose to extend the Yukawa sector by adding a $\mathbf{120}_H$ representation [11, 13, 16, 17].

In order to compare the parameters of a high-energy theory to low-energy observables, one must take into account the renormalization group equations (RGEs) [18]. Most previous analyses of fermion observables in SO(10) models use solutions of the RGEs for the SM to compare the parameters at the SO(10) breaking scale M_{GUT} to observables extrapolated from the experimental energy scale up to that scale [11, 12] or solve the RGEs for the parameter values from M_{GUT} down to the electroweak scale M_Z [13], assuming an SM-like model in the whole energy range. However, non-supersymmetric SO(10) models require an intermediate symmetry breaking [19], so it is worthwhile to consider a more complete analysis that takes into account the effects of an intermediate gauge group (ignoring it amounts to assuming that its effect is negligible, for example if the associated energy scale M_I of the intermediate symmetry breaking is very close to M_{GUT}). Various breaking chains are

possible which have different renormalization group (RG) running of the gauge couplings, resulting in different values for the energy scales M_I and M_{GUT} [20, 21]. A commonly considered intermediate symmetry is the Pati–Salam (PS) gauge group [22]. The derivation of the complete set of RGEs for the gauge, Yukawa, and scalar couplings [23–26] in such a breaking chain as well as their matching conditions at M_I was first attempted in ref. [27]. A numerical analysis based on the RGEs and matching conditions presented therein demonstrated the substantial effect that an intermediate gauge group in the symmetry breaking can have on the RG running and fits to fermion observables in a minimal SO(10) model [14]. This analysis was later refined by deriving correct RGEs and also considering an extended (or non-minimal) SO(10) model [17].

The present work aims to extend the analysis of the two models in refs. [14, 17] in several ways. Firstly, we fit to the two neutrino mass-squared differences separately, whereas the above mentioned works performed the fits to only their ratio. Secondly, we consider both normal ordering (NO) and inverted ordering (IO) of the neutrino masses. Thus we consider four different cases, namely two different models, each with both NO and IO. Lastly, we update the values of the observables at M_Z to the best-known values to date.

This paper is organized as follows. First, in section 2, we briefly describe the models including the breaking chain down to M_Z . Then in section 3, we describe the procedure used to perform the analysis. Next, in section 4, the results of the analysis are presented, discussed, and compared to previous results. Finally, in section 5, we summarize our findings and conclude.

2 Description of the minimal and extended models

In this section, we briefly outline the two models to which fits will be performed. More details on these models can be found in refs. [14, 17]. The two models are both non-supersymmetric and based on the SO(10) gauge group. In what follows, they are referred to as the *minimal model* and the *extended model* due to their difference in scalar representations (whether or not the $\mathbf{120}_H$ is included). We assume that the SO(10) symmetry breaking to the spontaneously broken SM in both models proceeds via the PS group, *viz.*

$$\begin{aligned} \text{SO}(10) &\xrightarrow{M_{\text{GUT}}} \text{SU}(4)_C \otimes \text{SU}(2)_L \otimes \text{SU}(2)_R \\ &\xrightarrow{M_I} \text{SU}(3)_C \otimes \text{SU}(2)_L \otimes \text{U}(1)_Y \\ &\xrightarrow{M_Z} \text{SU}(3)_C \otimes \text{U}(1)_{\text{em}}. \end{aligned} \tag{2.1}$$

The electroweak symmetry breaking scale is $M_Z = 91.1876 \text{ GeV}$ [28] and the energy scales of the other two symmetry breakings are computed to be [17]

$$M_I = 4.8 \cdot 10^{11} \text{ GeV} \quad \text{and} \quad M_{\text{GUT}} = 10^{16} \text{ GeV}, \tag{2.2}$$

respectively. These energy scales are uniquely derived from the requirement of gauge coupling unification at M_{GUT} with the coupling constants

$$\alpha_i^{-1}(M_{\text{GUT}}) \simeq \begin{cases} 37.0 & \text{(minimal model)} \\ 28.6 & \text{(extended model)} \end{cases}, \tag{2.3}$$

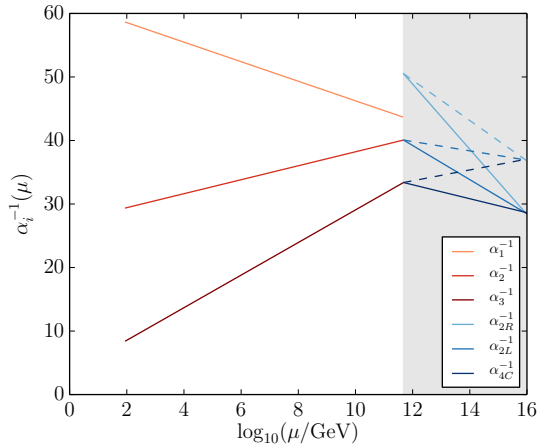


Figure 1: Gauge coupling unification in the minimal model (dashed curves) and extended model (solid curves). Below M_I , the RG running is the same. The shaded region, from M_I to M_{GUT} , denotes the energy interval of the intermediate gauge group.

as shown in figure 1, where the convention $\alpha_i = g_i^2/(4\pi)$ has been used. Note that we can perform this analysis independent of the RG running of the Yukawa couplings since, to one-loop order, the RGEs for the gauge couplings are independent of those of the Yukawa couplings [23, 24].

2.1 SO(10) Lagrangians

Above M_{GUT} , the Yukawa sector of the Lagrangian for the minimal model is given by

$$-\mathcal{L}_Y^{\text{GUT,min}} = \mathbf{16}_F(h\mathbf{10}_H + f\overline{\mathbf{126}}_H)\mathbf{16}_F, \quad (2.4)$$

where $\mathbf{16}_F$ is the spinor representation containing the fermions, whereas $\mathbf{10}_H$ and $\overline{\mathbf{126}}_H$ contain the Higgs scalars. Note that we forbid the coupling to the conjugate $\mathbf{10}_H^*$ by imposing a Peccei-Quinn $U(1)_{\text{PQ}}$ symmetry [4, 5]. In the extended model, we also include the $\mathbf{120}_H$ Higgs representation. Therefore, the Yukawa sector of the Lagrangian for this model is

$$-\mathcal{L}_Y^{\text{GUT,ext}} = \mathbf{16}_F(h\mathbf{10}_H + f\overline{\mathbf{126}}_H + g\mathbf{120}_H)\mathbf{16}_F. \quad (2.5)$$

The Yukawa couplings h , f , and g are 3×3 matrices in flavor space. For simplicity, one can choose a basis in which h is real and diagonal. The other two matrices f and g are then complex symmetric and complex antisymmetric, respectively.

2.2 Pati-Salam Lagrangians

Between M_{GUT} and M_I , the relevant fields decompose in the PS group as

$$\begin{aligned} \mathbf{16}_F &= (\mathbf{4}, \mathbf{2}, \mathbf{1}) \oplus (\overline{\mathbf{4}}, \mathbf{1}, \mathbf{2}) \equiv F_L \oplus F_R, \\ \mathbf{10}_H &= (\mathbf{1}, \mathbf{2}, \mathbf{2}) \oplus (\mathbf{6}, \mathbf{1}, \mathbf{1}), \\ \overline{\mathbf{126}}_H &= (\mathbf{6}, \mathbf{1}, \mathbf{1}) \oplus (\mathbf{10}, \mathbf{1}, \mathbf{3}) \oplus (\overline{\mathbf{10}}, \mathbf{3}, \mathbf{1}) \oplus (\mathbf{15}, \mathbf{2}, \mathbf{2}), \\ \mathbf{120}_H &= (\mathbf{10} + \overline{\mathbf{10}}, \mathbf{1}, \mathbf{1}) \oplus (\mathbf{6}, \mathbf{3}, \mathbf{1}) \oplus (\mathbf{6}, \mathbf{1}, \mathbf{3}) \oplus (\mathbf{15}, \mathbf{2}, \mathbf{2}) \oplus (\mathbf{1}, \mathbf{2}, \mathbf{2}). \end{aligned} \quad (2.6)$$

The fields that contribute to the particle masses are

$$\begin{aligned}
\Phi_{10} &\equiv (\mathbf{1}, \mathbf{2}, \mathbf{2})_{10}, & \Sigma_{126} &\equiv (\mathbf{15}, \mathbf{2}, \mathbf{2})_{126}, \\
\Phi_{120} &\equiv (\mathbf{1}, \mathbf{2}, \mathbf{2})_{120}, & \Sigma_{120} &\equiv (\mathbf{15}, \mathbf{2}, \mathbf{2})_{120}, \\
\bar{\Delta}_R &\equiv (\mathbf{10}, \mathbf{1}, \mathbf{3})_{126},
\end{aligned} \tag{2.7}$$

where the subscripts indicate which representation they originate from. Since these are the only scalars involved in the breaking chains, we appeal to the extended survival hypothesis to assume that they are the only ones that are present at this scale [12, 19, 29]. The Lagrangian for the minimal model between M_{GUT} and M_I is chosen as

$$-\mathcal{L}_Y^{\text{PS, min}} = Y_F^{(10)} \bar{F}_L \Phi_{10} F_R + Y_F^{(126)} \bar{F}_L \Sigma_{126} F_R + Y_R^{(126)} F_R^T C F_R \bar{\Delta}_R, \tag{2.8}$$

whereas for the extended model, we choose

$$\begin{aligned}
-\mathcal{L}_Y^{\text{PS, ext}} &= Y_F^{(10)} \bar{F}_L \Phi_{10} F_R + Y_F^{(126)} \bar{F}_L \Sigma_{126} F_R \\
&+ Y_R^{(126)} F_R^T C F_R \bar{\Delta}_R + Y_{F,1}^{(120)} \bar{F}_L \Phi_{120} F_R \\
&+ Y_{F,2}^{(120)} \bar{F}_L \Sigma_{120} F_R,
\end{aligned} \tag{2.9}$$

where C is the charge-conjugation matrix. The Yukawa coupling matrices $Y_F^{(10)}$, $Y_F^{(126)}$, $Y_R^{(126)}$, $Y_{F,1}^{(120)}$, and $Y_{F,2}^{(120)}$ are related to the ones appearing in the SO(10) Lagrangians by a set of matching conditions [20, 27, 30], for which we refer the reader to refs. [14, 17]. In ref. [17], the correct RGEs can also be found, which determine the evolution of the gauge and Yukawa couplings between M_{GUT} and M_I .

2.3 SM-like Lagrangian

Below M_I (and above M_Z), we assume as an SM-like model a two-Higgs-doublet model (2HDM), since this is embedded naturally into the PS model. The Lagrangian of the Yukawa sector is thus

$$-\mathcal{L}_Y^{2\text{HDM}} = Y_u \bar{q}_L \phi_2 u_R + Y_d \bar{q}_L \phi_1 d_R + Y_e \bar{\ell}_L \phi_1 e_R + Y_D \bar{\ell}_L \phi_2 N_R \tag{2.10}$$

for both the minimal and extended models. Here, q_L and ℓ_L are the quark and lepton $\text{SU}(2)_L$ doublets, respectively, and u_R , d_R , e_R , and N_R are the quark and lepton $\text{SU}(2)_L$ singlets, respectively. The coefficients Y_u , Y_d , Y_e , and Y_D are Yukawa matrices for the up-type quarks, down-type quarks, charged leptons, and neutrinos, respectively, and ϕ_1 and ϕ_2 are the two Higgs scalars. The vacuum expectation values (vevs), which are involved in the matching conditions for the Yukawa matrices [17], are denoted as

$$\begin{aligned}
k_{u,d} &= \langle \Phi_{10} \rangle_{u,d}, & v_{u,d} &= \langle \Sigma_{126} \rangle_{u,d}, & v_R &= \langle \bar{\Delta}_R \rangle, \\
z_{u,d} &= \langle \Phi_{120} \rangle_{u,d}, & t_{u,d} &= \langle \Sigma_{120} \rangle_{u,d},
\end{aligned} \tag{2.11}$$

where $\bar{\Delta}_R$ takes vev at M_I , while the others are $\text{SU}(2)_L$ doublets which take vev at M_Z . Note that similarly to ref. [17], we make the simplifying assumption that, although all

Energy region	Yukawa couplings	Scalar fields
$M_{\text{GUT}} < \mu$	h, f, g	$\mathbf{10}_H, \overline{\mathbf{126}}_H, \mathbf{120}_H$
$M_I < \mu < M_{\text{GUT}}$	$Y_F^{(10)}, Y_F^{(126)}, Y_R^{(126)},$ $Y_{F,1}^{(120)}, Y_{F,2}^{(120)}$	$\Phi_{10}, \Sigma_{126}, \Phi_{120},$ $\Sigma_{120}, \overline{\Delta}_R$
$M_Z < \mu < M_I$	Y_u, Y_d, Y_e, Y_D	ϕ_1, ϕ_2

Table 1: Summary of relevant Yukawa couplings and scalar fields in each energy region.

$SU(2)_L$ doublet scalars contribute to the fermion masses, the Higgs doublets ϕ_1 and ϕ_2 consist predominantly of the two doublet scalars originating in Φ_{10} . The constraint on the vevs can therefore be approximated to $\sqrt{k_u^2 + k_d^2} = 246 \text{ GeV}$ [31]. A more complete analysis of the scalar potential is needed to determine the composition of ϕ_1 and ϕ_2 in terms of the available scalars and may result in a different constraint on the vevs. However, this is beyond the scope of our work and we make the assumption that the dominant contributions to ϕ_1 and ϕ_2 come from Φ_{10} .

The RGEs for the evolution of the gauge and Yukawa couplings have previously been presented in the literature [17, 27]. For neutrino masses, we assume a type-I seesaw mechanism with the seesaw scale close to M_I . Thus, we have an effective neutrino mass matrix

$$m_\nu = M_D^T M_R^{-1} M_D, \quad (2.12)$$

where $M_D = (k_u/\sqrt{2})Y_D$ is the Dirac neutrino mass matrix and M_R is the right-handed Majorana neutrino mass matrix. For more details on its relation to the Yukawa couplings in the PS model as well as details regarding the RG running of neutrino parameters, the reader is referred to ref. [17]. As explained therein, we also need to include a Higgs self-coupling for each Higgs doublet, since they affect the RG running of the neutrino mass matrix [32, 33]. However, as in ref. [17], we assume that the quartic couplings that involve cross-couplings between the two Higgs doublets are zero, so that we have the scalar potential $V(\phi_1, \phi_2) = \lambda_1(\phi_1^\dagger \phi_1)^2 + \lambda_2(\phi_2^\dagger \phi_2)^2$.

A summary of the relevant quantities in the different energy regions is presented in table 1. At each symmetry breaking scale, the Yukawa couplings of the lower energy theory are linear combinations of those of the higher energy theory. The quantities that exhibit RG running — *and therefore change with energy* — in the PS model are the Yukawa couplings in $M_I < \mu < M_{\text{GUT}}$ as well as the gauge couplings. In the 2HDM, the quantities that exhibit RG running — *and therefore change with energy* — are the Yukawa couplings in $M_Z < \mu < M_I$ as well as the effective neutrino mass matrix, gauge couplings, and Higgs quartic couplings. The only vevs that we consider are those that contribute to the fermion masses, which are listed in eq. (2.11). All except v_R are vevs of $SU(2)_L$ doublet scalars which take vevs at M_Z , but enter as effective parameters in the matching of Yukawa couplings at M_I . We assume that the vevs are constant in energy.

3 Parameter-fitting procedure

In this section, we describe the procedure and numerical tools used to perform the parameter fits, which follows closely refs. [14, 17]. The general procedure consists of minimizing a χ^2 function, which is formed by comparing measured data at M_Z with the RG running of parameter values from M_{GUT} to M_Z in a given SO(10) model. This RG running is performed by solving the relevant RGEs of the model parameters from M_{GUT} to M_Z , taking into account the change of parameters at M_I . Due to the nature of the matching conditions at M_I , it is not possible to extrapolate the observables from M_Z to M_{GUT} and we are forced to perform the RG running from the high-energy model down to the low-energy observables. Note that due to the intermediate PS symmetry, the parameters for which the RGEs are solved above M_I are not the Yukawa couplings that appear in the SM, but rather the Yukawa couplings $Y_F^{(10)}$, $Y_F^{(126)}$, $Y_R^{(126)}$, $Y_{F,1}^{(120)}$, and $Y_{F,2}^{(120)}$ of the PS model. In the minimal model, there are 22 parameters: three in h , twelve in f , four in the complex vevs v_u and v_d , one in the ratio of the real vevs k_u/k_d , one in the real vev v_R , and one in the Higgs self-coupling λ (since the two are assumed to be equal above M_I). The extended model has a total of 34 parameters, which are the 22 of the minimal model and an extra twelve: six in g , four in the complex vevs t_u and z_u , and two in the real vevs t_d and z_d .

In order to determine the values of the above-mentioned parameters that provide the best fit to measured data, we employ the following strategy:

1. Generate the parameter values at M_{GUT} .
2. Numerically solve the one-loop RGEs of the parameters that exhibit RG running to relate the parameter values at M_{GUT} to those at M_Z . At M_I , use the matching conditions to transform the parameters to the ones that are relevant in the lower energy region.
3. Construct the 18 fermion observables (masses and mixing parameters) at M_Z and compare these to measured data by calculating the corresponding value of the χ^2 function.
4. Repeat the above steps to find the parameter values that provide the best fit and the corresponding value of the χ^2 function.

The χ^2 function is defined as

$$\chi^2 = \sum_{i=1}^N \left(\frac{\mu_i - X_i}{\sigma_i} \right)^2 \equiv \sum_{i=1}^N p_i^2, \quad (3.1)$$

where X_i is the measured value of the i th observable at M_Z with corresponding error σ_i and μ_i is the corresponding predicted value of the given model for the current choice of parameter values. We also define the pulls p_i as above for later convenience. For the sampling of the parameters, we interchangeably use the packages MultiNest [34–36], which is a nested sampling algorithm, and Diver [37], which is a differential evolution algorithm. Prior distributions are used to generate the next iteration of parameter values such that

Observable	X_i	σ_i	σ_i/X_i
m_d [GeV]	$2.71 \cdot 10^{-3}$	$1.4 \cdot 10^{-3}$	50 %
m_s [GeV]	0.0553	0.017	30 %
m_b [GeV]	2.86	0.086	3 %
m_u [GeV]	$1.27 \cdot 10^{-3}$	$6.4 \cdot 10^{-4}$	50 %
m_c [GeV]	0.634	0.10	15 %
m_t [GeV]	171	3.5	2 %
$\sin \theta_{12}^q$	0.225	$2.3 \cdot 10^{-3}$	1 %
$\sin \theta_{13}^q$	$3.57 \cdot 10^{-3}$	$3.6 \cdot 10^{-4}$	10 %
$\sin \theta_{23}^q$	0.0411	$1.3 \cdot 10^{-3}$	3 %
δ_{CKM}	1.24	0.062	5 %
m_e [GeV]	$4.87 \cdot 10^{-4}$	$2.4 \cdot 10^{-5}$	5 %
m_μ [GeV]	0.103	$5.1 \cdot 10^{-3}$	5 %
m_τ [GeV]	1.75	0.087	5 %
Δm_{21}^2 [eV ²]	$7.40 \cdot 10^{-5}$	$6.7 \cdot 10^{-6}$	9 %
Δm_{31}^2 [eV ²] (NO)	$2.49 \cdot 10^{-3}$	$7.5 \cdot 10^{-5}$	3 %
Δm_{32}^2 [eV ²] (IO)	$-2.47 \cdot 10^{-3}$	$7.4 \cdot 10^{-5}$	3 %
$\sin^2 \theta_{12}^\ell$	0.307	0.013	4 %
$\sin^2 \theta_{13}^\ell$ (NO)	0.0221	$7.5 \cdot 10^{-4}$	3 %
$\sin^2 \theta_{13}^\ell$ (IO)	0.0223	$7.4 \cdot 10^{-4}$	3 %
$\sin^2 \theta_{23}^\ell$ (NO)	0.538	0.069	13 %
$\sin^2 \theta_{23}^\ell$ (IO)	0.554	0.033	6 %

Table 2: Mean values of the 18 observables and corresponding errors at the electroweak scale M_Z . The label NO (IO) denotes the parameter values of normal (inverted) neutrino mass ordering. Mean values of the quark and charged-lepton masses are based on updated calculations of refs. [39, 40] and mean values of the quark mixing parameters are computed from values given in ref. [28]. The neutrino mass-squared differences and the leptonic mixing angles are taken from refs. [41, 42].

the elements of h , f , and g are sampled from logarithmic priors between 10^{-20} and 10^{-1} (and allowed to be negative), λ is sampled from a uniform prior between -1 and 1 , and the vevs are sampled from uniform priors between -550 GeV and 550 GeV, except for ν_R which is sampled from a uniform prior between 10^{12} GeV and 10^{16} GeV (this departure from the extended survival hypothesis is necessary to reproduce the neutrino mass-squared differences). The ratio k_u/k_d which is sampled from a uniform prior between -550 and 550 . The ranges of the above-mentioned priors are obtained from their expected orders of magnitude as well as preliminary numerical tests. After the sampling algorithm has converged on a set of parameter values, a Nelder-Mead simplex algorithm [38] is used to further evolve the parameter values to a set that provides an even better fit. However, note that one can never be sure that the global minimum is found. The best that one can do is to restart the minimization procedure several times with different starting parameter values.

In table 2, we list the measured values of the 18 observables that we fit to. Some

Neutrino mass ordering	Minimal model	Extended model
NO	85.9	18.6
IO	1424	3081

Table 3: Values of the χ^2 function corresponding to the best fits for the two models and for both normal (NO) and inverted (IO) neutrino mass ordering.

comments regarding the choice of values and their corresponding errors are in order. Firstly, the values of the quark and charged-lepton masses are taken from an updated RG running analysis, using the same method as in refs. [39, 40]. The relative errors of the quark masses are set to values between 50 % (up and down quarks) and 2 % (top quark), motivated by large theoretical uncertainties in the quark masses, whereas the charged-lepton masses have relative errors set to 5 %, due to their almost negligible experimental errors, since otherwise their small errors render the fit practically impossible. Secondly, the values of the quark mixing angles are calculated from the elements of the Cabibbo-Kobayashi-Maskawa (CKM) matrix given in ref. [28], whereas the Dirac CP-violating phase of the CKM matrix is computed from the Wolfenstein parameters of the same reference. The chosen relative errors between 1 % and 10 % reflect the relation among the uncertainties of the quark mixing parameters. Finally, the values of the leptonic mixing angles and the neutrino mass-squared differences are taken from refs. [41, 42], as are the associated errors of the leptonic mixing angles. For the mass-squared differences, we choose the relative errors so that their ratio has a relative error of 10 %, since the neutrino mass-squared differences have larger uncertainties than the charged-lepton masses. Note that we do not fit to the leptonic Dirac CP-violating phase, since knowledge of its value is limited to indications from global fits, see for example refs. [41, 42].

4 Results and discussion

The χ^2 minimization procedure resulted in only one of the four cases having an acceptable fit, namely the extended model with NO, as shown in table 3. For this case, the numerical values of the matrices h , f , and g corresponding to the minimum value of the χ^2 function are

$$\begin{aligned}
h &= \begin{pmatrix} -1.37 \cdot 10^{-6} & 0 & 0 \\ 0 & -1.31 \cdot 10^{-3} & 0 \\ 0 & 0 & 0.300 \end{pmatrix}, \\
f &= \begin{pmatrix} 6.41 \cdot 10^{-19} - 1.32 \cdot 10^{-25}i & 6.60 \cdot 10^{-6} + 1.17 \cdot 10^{-15}i & -4.82 \cdot 10^{-5} - 4.77 \cdot 10^{-14}i \\ 6.60 \cdot 10^{-6} + 1.17 \cdot 10^{-15}i & -1.05 \cdot 10^{-4} - 6.36 \cdot 10^{-5}i & 1.33 \cdot 10^{-12} - 1.98 \cdot 10^{-3}i \\ -4.82 \cdot 10^{-5} - 4.77 \cdot 10^{-14}i & 1.33 \cdot 10^{-12} - 1.98 \cdot 10^{-3}i & -4.16 \cdot 10^{-12} - 7.15 \cdot 10^{-4}i \end{pmatrix}, \\
g &= \begin{pmatrix} 0 & -1.58 \cdot 10^{-7} - 1.22 \cdot 10^{-6}i & 1.40 \cdot 10^{-14} + 1.18 \cdot 10^{-17}i \\ 1.58 \cdot 10^{-7} + 1.22 \cdot 10^{-6}i & 0 & 3.90 \cdot 10^{-3} + 3.79 \cdot 10^{-13}i \\ -1.40 \cdot 10^{-14} - 1.18 \cdot 10^{-17}i & -3.90 \cdot 10^{-3} - 3.79 \cdot 10^{-13}i & 0 \end{pmatrix},
\end{aligned} \tag{4.1}$$

and the values of the remaining parameters are given in table 4.

Parameter	Best-fit value
k_u/k_d	65.5
v_u [GeV]	$0.0 + 4.91i$
v_d [GeV]	$0.0 - 110i$
t_u [GeV]	$-666 + 0.0i$
t_d [GeV]	-149
z_u [GeV]	$0.0 + 105i$
z_d [GeV]	56.6
λ	0.0
v_R [GeV]	$5.51 \cdot 10^{13}$

Table 4: Parameter values of the extended model with normal neutrino mass ordering corresponding to the minimum value of the χ^2 function.

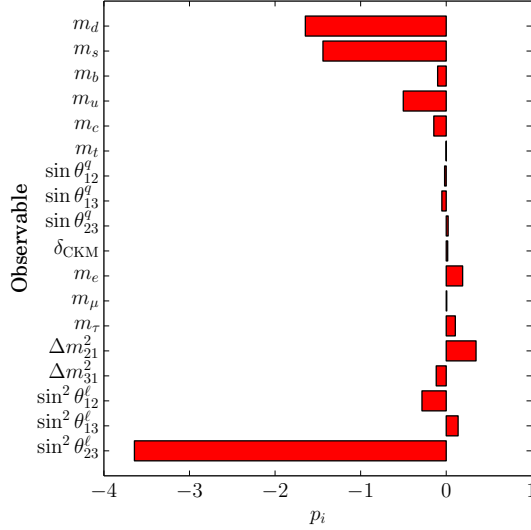


Figure 2: Pulls p_i for each observable in the extended model with normal neutrino mass ordering, given the set of parameter values that has the minimum value of the χ^2 function.

In figure 2, the pulls p_i for each observable, defined in eq. (3.1), are displayed. The sum of the squares of the pulls is the χ^2 function. It is evident that the largest contribution to the χ^2 function is due to the observable $\sin^2 \theta_{23}^l$, for which the obtained prediction from the best-fit parameters is 0.287 (corresponding to $\theta_{23}^l \simeq 32.4^\circ$ in the lower octant), which is significantly lower than the measured value of 0.538 (corresponding $\theta_{23}^l \simeq 47.2^\circ$ in the higher octant). This tension due to the octant of θ_{23}^l was also noted in a previous fit to observables at M_{GUT} [12]. In fact, the measured value of $\sin^2 \theta_{23}^l$ used in the minimization procedure comes from a global fit [41, 42] and although the 1σ range does not include our predicted value, it does allow for θ_{23}^l in the lower octant. Furthermore, previous versions of the global fit [41, 43] predicted a value of θ_{23}^l in the lower octant, which was used in a fit similar to ours presented in ref. [17]. Replacing the present measured value of $\sin^2 \theta_{23}^l$

by its previous value of 0.441, the χ^2 function for our current best-fit parameters takes the value 10.4, which is lower than the value 11.2 presented in ref. [17]. Furthermore, we agree with their conclusion that significant tension in the fit is caused by the masses of the down and strange quarks.

Since the fit to the minimal model with NO is not totally unacceptable, it is worth to consider the significant contributions to its χ^2 function. The largest contribution comes from $\sin^2 \theta_{12}^\ell$, followed by $\sin^2 \theta_{23}^\ell$. In absolute terms, the best-fit value of $\sin^2 \theta_{12}^\ell$ is closer to the measured value than what is the case for $\sin^2 \theta_{23}^\ell$, but since the relative error of the former is much smaller than that of the latter, it gives a larger contribution to the value of its χ^2 function. Similarly to the extended model, the best-fit parameter values of this model also predict a value of θ_{23}^ℓ in the lower octant.

In figure 3, the RG running of the fermion observables (except the quark mixing parameters since they exhibit small RG running) from M_{GUT} down to M_Z for the best-fit parameter values of extended model with NO are presented, with the dashed curves showing the RG running without the intermediate gauge group. That is, assuming the SM-like model discussed in section 2.3 for the whole energy range and with the same best-fit parameter values at M_{GUT} . Note that since particle mass states are not well defined before electroweak symmetry breaking, the parameters above M_Z are to be considered as effective parameters of the model. They are computed by applying the matching conditions to the parameters of the PS model in order to transform them to the parameters of the 2HDM from which the observables can be calculated. It is evident that the intermediate gauge group has a significant effect on the RG running. The quark masses display a diverging trend as the energy scale decreases from M_{GUT} in the case of no intermediate gauge group. In fact, the parameters diverge so that the system of equations has no solution below a certain energy (which is why the dashed curves do not cover the full energy range even for the other observables). For the charged-lepton masses, the leptonic mixing angles, and the neutrino mass-squared differences, the difference in slope between the PS and 2HDM models is more pronounced. Particularly, the leptonic mixing angles exhibit large RG running in the PS model, but almost no RG running in the 2HDM model.

As a consistency check, one can observe that the RG running below M_I in the case of an intermediate gauge group is of a similar form as that without an intermediate gauge group (since it is the same equations that are being solved in these two cases, with different initial conditions). With the intermediate gauge group, the diverging effect is offset to lower energies so that the divergence does not occur within the energy region under study, since the RGEs of the 2HDM are applied over a smaller energy range than if there were no intermediate gauge group. In fact, if one extends the RG running to energies well below M_Z , the diverging behavior occurs at a lower energy scale.

In order to describe the general behaviour of the RG running, particularly the quark and charged-lepton masses since these are linear in the Yukawa couplings, one can approximate the RGEs listed in ref. [17], by their leading terms. For the energy region between M_{GUT} and M_I , the leading term is in all cases the one involving the gauge couplings. To

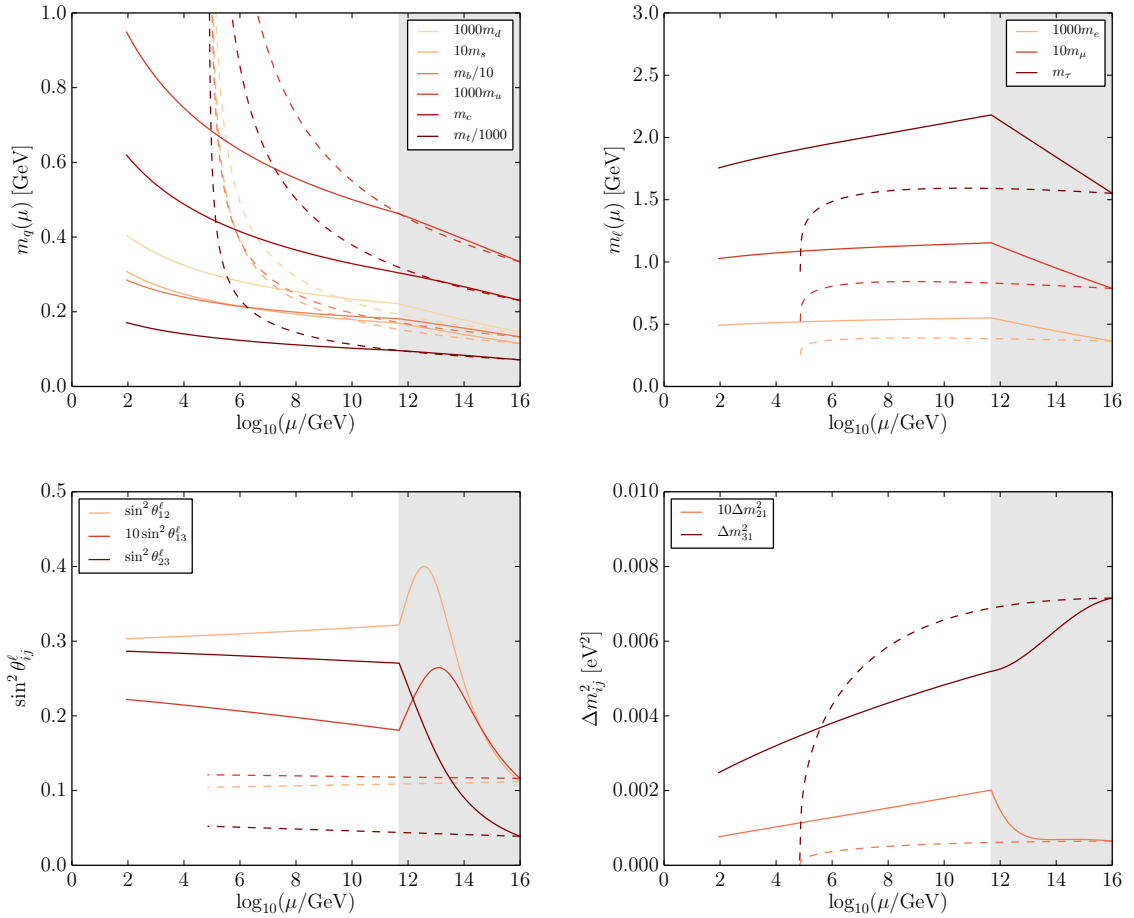


Figure 3: RG running of the quark masses (upper left panel), charged-lepton masses (upper right panel), leptonic mixing angles (lower left panel), and neutrino mass-squared differences (lower right panel) in the extended model with normal neutrino mass ordering. The solid (dashed) curve shows the RG running with (without) the intermediate gauge group between M_{GUT} and M_1 , denoted by the shaded area.

an accuracy of a few percent, the RGEs can be approximated by

$$16\pi^2 \frac{dY_i}{dt} \simeq f_i(g_j(t))Y_i(t), \quad (4.2)$$

where $t = \ln(\mu/\text{GeV})$, the subscript i denotes the Yukawa coupling matrix in question and f_i denotes a function of the three gauge couplings g_j . The same applies to the RGEs in the 2HDM model for Y_u and Y_d , but for Y_e the leading term is the one involving Y_d such that the RGE may be approximated by

$$16\pi^2 \frac{dY_e}{dt} \simeq 3\text{tr}(Y_d(t)^\dagger Y_d(t))Y_e(t). \quad (4.3)$$

In the energy region below M_1 , the approximation is not quite as good with the error of the charged-fermion masses at M_Z between 10 % and 30 %. The fact that the RGEs for the quark and charged-lepton Yukawa matrices have different leading terms explains

why the masses exhibit such different RG running. The mixing parameters and neutrino mass-squared differences cannot be well approximated by the leading terms, since these observables are related to the Yukawa couplings in a more complicated and non-linear way.

The other two works that take into account the effect of the intermediate gauge group, refs. [14, 17], agree with our conclusion that it has a significant effect on the RG running of the parameters and thus on the fit itself. However, we find a considerably different behavior of the RG running of the parameters as well as increased difficulty in fitting the SO(10) models to the data. Comparing the effect of the intermediate gauge group on the RG running in our work with that of ref. [17], we find a considerably closer similarity between the RG running behaviour of the parameters below M_I with that in the absence of an intermediate gauge group. In comparison to ref. [11], they, like us, concluded that the easiest model to fit to (out of the ones considered above) is the extended model with NO, in agreement also with ref. [13]. The latter work also found that IO is more difficult to fit to than NO. However, they could find considerably better fits than we have found in all cases, since they do not take into account the intermediate gauge group, which increases the complexity of the problem considerably and complicates the fit. Of course, it must be noted that we cannot ensure that we have found the global minimum and cannot with complete certainty rule out the other three cases for which no acceptable fit was found. Furthermore, there may be other effects which may act to improve the ability to fit the models to the measured values of the observables, such as higher-order terms in the RGEs and threshold corrections to the RG running [15]. Other corrections may also arise from variations in some of the assumptions regarding the SM-like model. Such corrections may be particularly interesting for the minimal model with normal neutrino mass hierarchy, since this case is not too far from having a reasonable fit. One possibility may be to include the effects of type-II seesaw, particularly since the most tension was found in the leptonic mixing sector.

5 Summary and conclusions

We have performed numerical fits to two different non-SUSY SO(10) models, namely the minimal model and the extended model, which differ by the inclusion of a $\mathbf{120}_H$ representation in the Yukawa sector of the Lagrangian. The fits were performed with both NO and IO, and assuming a type-I seesaw mechanism for neutrino mass generation. The results of the fits show that out of the four cases considered, only the extended model with NO is viable with $\chi^2 \simeq 18.6$. One reason for the difficulty in finding acceptable fits of the models is the extra complexity introduced by the intermediate gauge group, which has been shown to have a considerable effect on the RG running as can be seen from the change in slope at M_I in figure 3. Another reason for the difficulty in the fitting procedure is the fact that the best-known value of θ_{23}^l is now in the higher octant, whereas a value in the lower octant (as previously predicted) would considerably improve the fit. However, before definitely ruling out the three cases that were unable to accommodate the measured values of the observables at M_Z , one should investigate the effects of higher-order terms as well as threshold corrections.

Acknowledgments

We would like to thank Sofiane Boucenna, Davide Meloni, Stella Riad, and Shun Zhou for useful discussions. T.O. acknowledges support by the Swedish Research Council (Vetenskapsrådet) through contract No. 2017-03934 and the KTH Royal Institute of Technology for a sabbatical period at the University of Iceland. M.P. thanks “Stiftelsen Olle Engkvist Byggmästare” and “Roland Gustafssons Stiftelse för teoretisk fysik” for financial support. Numerical computations were performed on resources provided by the Swedish National Infrastructure for Computing (SNIC) at PDC Center for High Performance Computing (PDC-HPC) at KTH Royal Institute of Technology in Stockholm, Sweden under project number PDC-2017-115.

References

- [1] H. Georgi, *Stud. Nat. Sci.* **9**, 329 (1975).
- [2] H. Fritzsch and P. Minkowski, *Annals Phys.* **93**, 193 (1975).
- [3] J. A. Harvey, D. B. Reiss, and P. Ramond, *Nucl. Phys.* **B199**, 223 (1982).
- [4] K. S. Babu and R. N. Mohapatra, *Phys. Rev. Lett.* **70**, 2845 (1993), [arXiv:hep-ph/9209215 \[hep-ph\]](#).
- [5] B. Bajc, A. Melfo, G. Senjanović, and F. Vissani, *Phys. Rev.* **D73**, 055001 (2006), [arXiv:hep-ph/0510139 \[hep-ph\]](#).
- [6] E. Witten, *Phys. Lett.* **91B**, 81 (1980).
- [7] K. Matsuda, Y. Koide, and T. Fukuyama, *Phys. Rev.* **D64**, 053015 (2001), [arXiv:hep-ph/0010026 \[hep-ph\]](#).
- [8] K. Matsuda, Y. Koide, T. Fukuyama, and H. Nishiura, *Phys. Rev.* **D65**, 033008 (2002), [Erratum: *Phys. Rev.*D65,079904(2002)], [arXiv:hep-ph/0108202 \[hep-ph\]](#).
- [9] T. Fukuyama and N. Okada, (2018), [arXiv:1802.06530 \[hep-ph\]](#).
- [10] S. Bertolini, T. Schwetz, and M. Malinský, *Phys. Rev.* **D73**, 115012 (2006), [arXiv:hep-ph/0605006 \[hep-ph\]](#).
- [11] A. S. Joshipura and K. M. Patel, *Phys. Rev.* **D83**, 095002 (2011), [arXiv:1102.5148 \[hep-ph\]](#).
- [12] G. Altarelli and D. Meloni, *J. High Energy Phys.* **08**, 021 (2013), [arXiv:1305.1001 \[hep-ph\]](#).
- [13] A. Dueck and W. Rodejohann, *J. High Energy Phys.* **09**, 024 (2013), [arXiv:1306.4468 \[hep-ph\]](#).
- [14] D. Meloni, T. Ohlsson, and S. Riad, *J. High Energy Phys.* **12**, 052 (2014), [arXiv:1409.3730 \[hep-ph\]](#).
- [15] K. S. Babu and S. Khan, *Phys. Rev.* **D92**, 075018 (2015), [arXiv:1507.06712 \[hep-ph\]](#).
- [16] K. S. Babu, B. Bajc, and S. Saad, *J. High Energy Phys.* **02**, 136 (2017), [arXiv:1612.04329 \[hep-ph\]](#).
- [17] D. Meloni, T. Ohlsson, and S. Riad, *J. High Energy Phys.* **03**, 045 (2017), [arXiv:1612.07973 \[hep-ph\]](#).
- [18] T. Ohlsson and S. Zhou, *Nature Commun.* **5**, 5153 (2014), [arXiv:1311.3846 \[hep-ph\]](#).

- [19] F. del Aguila and L. E. Ibáñez, *Nucl. Phys.* **B177**, 60 (1981).
- [20] N. G. Deshpande, E. Keith, and P. B. Pal, *Phys. Rev.* **D46**, 2261 (1993).
- [21] S. Bertolini, L. Di Luzio, and M. Malinský, *Phys. Rev.* **D80**, 015013 (2009), [arXiv:0903.4049 \[hep-ph\]](https://arxiv.org/abs/0903.4049).
- [22] J. C. Pati and A. Salam, *Phys. Rev.* **D10**, 275 (1974), [Erratum: *Phys. Rev.* **D11**, 703 (1975)].
- [23] D. R. T. Jones, *Phys. Rev.* **D25**, 581 (1982).
- [24] M. E. Machacek and M. T. Vaughn, *Nucl. Phys.* **B222**, 83 (1983).
- [25] M. E. Machacek and M. T. Vaughn, *Nucl. Phys.* **B236**, 221 (1984).
- [26] M. E. Machacek and M. T. Vaughn, *Nucl. Phys.* **B249**, 70 (1985).
- [27] T. Fukuyama and T. Kikuchi, *Mod. Phys. Lett.* **A18**, 719 (2003), [arXiv:hep-ph/0206118 \[hep-ph\]](https://arxiv.org/abs/hep-ph/0206118).
- [28] C. Patrignani *et al.* (Particle Data Group), *Chin. Phys.* **C40**, 100001 (2016).
- [29] S. Dimopoulos and H. M. Georgi, *Phys. Lett.* **140B**, 67 (1984).
- [30] L. J. Hall, *Nucl. Phys.* **B178**, 75 (1981).
- [31] G. C. Branco, P. M. Ferreira, L. Lavoura, M. N. Rebelo, M. Sher, and J. P. Silva, *Phys. Rept.* **516**, 1 (2012), [arXiv:1106.0034 \[hep-ph\]](https://arxiv.org/abs/1106.0034).
- [32] S. Antusch, M. Drees, J. Kersten, M. Lindner, and M. Ratz, *Phys. Lett.* **B525**, 130 (2002), [arXiv:hep-ph/0110366 \[hep-ph\]](https://arxiv.org/abs/hep-ph/0110366).
- [33] W. Grimus and L. Lavoura, *Eur. Phys. J.* **C39**, 219 (2005), [arXiv:hep-ph/0409231 \[hep-ph\]](https://arxiv.org/abs/hep-ph/0409231).
- [34] F. Feroz and M. P. Hobson, *Mon. Not. Roy. Astron. Soc.* **384**, 449 (2008), [arXiv:0704.3704 \[astro-ph\]](https://arxiv.org/abs/0704.3704).
- [35] F. Feroz, M. P. Hobson, and M. Bridges, *Mon. Not. Roy. Astron. Soc.* **398**, 1601 (2009), [arXiv:0809.3437 \[astro-ph\]](https://arxiv.org/abs/0809.3437).
- [36] F. Feroz, M. P. Hobson, E. Cameron, and A. N. Pettitt, (2013), [arXiv:1306.2144 \[astro-ph.IM\]](https://arxiv.org/abs/1306.2144).
- [37] G. D. Martinez, J. McKay, B. Farmer, P. Scott, E. Roebber, A. Putze, and J. Conrad (GAMBIT), *Eur. Phys. J.* **C77**, 761 (2017), [arXiv:1705.07959 \[hep-ph\]](https://arxiv.org/abs/1705.07959).
- [38] W. H. Press, S. A. Teukolsky, W. T. Vetterling, and B. P. Flannery, *Numerical Recipes in FORTRAN: The Art of Scientific Computing* (Cambridge University Press, 1992).
- [39] Z.-z. Xing, H. Zhang, and S. Zhou, *Phys. Rev.* **D77**, 113016 (2008), [arXiv:0712.1419 \[hep-ph\]](https://arxiv.org/abs/0712.1419).
- [40] Z.-z. Xing, H. Zhang, and S. Zhou, *Phys. Rev.* **D86**, 013013 (2012), [arXiv:1112.3112 \[hep-ph\]](https://arxiv.org/abs/1112.3112).
- [41] I. Esteban, M. C. Gonzalez-Garcia, M. Maltoni, I. Martinez-Soler, and T. Schwetz, *J. High Energy Phys.* **01**, 087 (2017), [arXiv:1611.01514 \[hep-ph\]](https://arxiv.org/abs/1611.01514).
- [42] NuFIT3.2, www.nu-fit.org/?q=node/166 (2018).
- [43] NuFIT3.0, www.nu-fit.org/?q=node/139 (2016).